Simplified AltBOC Receiver Performance Analysis

Rui Filipe Duarte Nunes
ruifdn@gmail.com

Instituto Superior Técnico, Lisboa, Portugal

May 2016

Abstract

The E5 AltBOC signal is a complex and exotic transmission signal used in Galileo satellites to enable the computation of a precise value for the receiver position. Since it is relatively new, there is a lot of unexplored terrain regarding this subject namely the receiver architecture that best suits the problem. This work addresses implementation aspects of an E5 AltBOC receiver ready to demodulate data from both bands E5a and E5b together as Dual SideBand (DSB) or separately as Single SideBand (SSB) and compare its results. This work focus its research on the tracking process where a Doppler frequency and code delay must be aligned between the local generated replica and the received signal to operate properly. The innovating part of this thesis is the implementation of a Dual Side Band receiver that uses complex correlators in its architecture that can process simultaneously the information of both E5a and E5b data and pilot channels. In the results chapter of this document, we present the comparative results between DSB and SSB for various conditions including the variation of the carrier-to-noise parameter.
Keywords: Galileo, E5 Signal, AltBOC modulation, Receiver, Tracking

1. Introduction

Galileo is the European Global Navigation Satellite System (GNSS) and provides a highly accurate, guaranteed global positioning service under civilian control [17]. The European GNSS approach began with the European Geostationary Navigation Overlay (EGNOS), which provides civil complements to GPS since mid-2005 in its initial operation. From the very beginning, EGNOS was meant to be the bridge to Europe's own full-fledged GNSS.

1.1. State-of-the-art

Galileo uses 3 different bands; band E5 is the one with the lowest central frequency (f_c = 1191.795 MHz) but exhibits the widest bandwidth. The modulation assigned to this band, the AltBOC(15,10), is a complex signal composed of 4 codes multiplexed so as to have a constant envelope. This is the most sophisticated and promising signal that is transmitted by the Galileo system. The main lobes of the signal spans over 50 MHz which makes the AltBOC bandwidth the largest of all GNSS signals. As a consequence, the receiver desiring to receive the complete signal shall have a bandwidth about thirty times larger than the current basic GPS receivers. AltBOC was at first imagined to fulfil a need: be able to generate and multiplex 2 or 4 navigation signal components (each with its own PRN code) or two close frequency bands taking into account the limitations of the onboard output multiplexer (OMUX), and giving it a constant envelope in order to maximize the amplifier efficiency. Processing the whole signal rather than the 2 separate E5a and E5b signals wasn't envisioned at first. The idea of receiving the complete AltBOC arrived later when it was understood that processing this wideband signal would lead to unprecedented tracking accuracy not only in Gaussian channels but also in the presence of multipath. This advantage was later confirmed by measurements performed on the real signal broadcasted by GIOVE-A [8].

For the single carrier approach with baseband multiplexing of 4 different signals in E5-band, candidate modulation schemes are Complex-LOC(15,10), Complex-BOC(15,10) and the constant envelope method of AltBOC(15,10) which are explained and compared in [15]. In order to analyze DSB and SSB tracking accuracy of such signals the concept of complex baseband receiver model with a non-coherent DLL is considered therein.

Some of the first architectures proposed to track AltBOC signals were described in the patents [5] and [18]. In general, the receiver designer can choose among 4 options for processing the E5 signal, or any AltBOC signal (for instance, in Beidou systems): (i) process the entire E5 signal as a wideband 8-phase signal; (ii) process both E5a and E5b, but separately; (iii) process only the E5a component,

and (iv) process only the E5b signal.

In [14], several aspects of the AltBOC receiver were discussed and it was shown that, due to the large bandwidth of the signals, some problems, namely signal distortion, might appear in the presence of strong ionospheric electron density. The limitations imposed by the ionosphere on the processing of wideband signals were addressed in more depth in [4].

The analysis of the possible architectures allowed by the AltBOC signals is carried out in [9] with a new architecture being proposed and discussed (see also [10]). This effort was further developed in [13] where the candidate discusses new acquisition, tracking and multipath mitigation algorithms.

More recent research analyzes the potential of the combination of Galileo E1 CBOC and E5 AltBOC pseudoranges for surveying and mapping applications. The tracking precision of the E1 and E5 pseudoranges under "open sky" and strong "tree coverage" scenarios result in 0.25 to 2.0 m (E1) and 0.02 to 0.08 m (E5) pseudorange precisions. These values permit the pseudorange solutions to compete with carrier phase solutions for certain types of applications that require precisions around 10 cm. The main advantages of pseudorange positioning are the simplicity and robustness of data processing [2]. One of the promising applications of AltBOC signals is in precise automobile navigation; however, this application will be viable only after a sufficient number of Galileo satellites are deployed, which is expected to happen in the next four-six years [16].

1.2. Objectives

The objective of this work is to simulate and test the robustness of a Galileo E5 AltBOC receiver using the Dual Side Band (DSB) and Single Side Band (SSB) signal data processing methods and compare their results.

The robustness of the algorithms is tested by decreasing the value of the carrier-to-noise ratio for different combinations of parameters such as code discriminator Early(E)-Late(L) spacing, Phase Lock Loop (PLL) and Delay Lock Loop (DLL) noise equivalent bandwidths, etc.

Another objective is to calibrate and optimize the receiver simulated parameters in order to achieve the best results.

2. Implementation

An AltBOC receiver, based on the coherent reception and processing of the entire Galileo E5 band, was proposed in [10] and is shown in fig. 1. This receiver will be herein analyzed.

3. Results

The simulated receiver is fully implemented in Matlab.

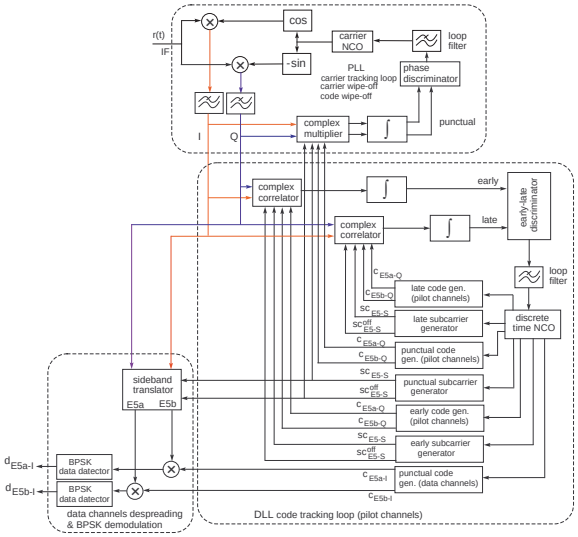

Figure 1: Block diagram of the dual band receiver architecture for Galileo AltBOC signals [10]

3.1. Monte Carlo Simulation Aspects

An important question to be answered within the context of the Monte Carlo simulation is how many runs are necessary to evaluate the receiver performance variable X (for instance, the DLL rms code error) with regard to a certain parameter S, such as $S = C/N_0$. The immediate solution is: the larger the number of runs the better. However, the user is faced with a tradeoff between run time and statistical variability [6]. In fact, simulation is computationally expensive because the required sampling rate of the AltBOC signals to meet the Nyquist criterion is very high, typically > 50 Msamples/s and the brute force solution is, in general, prohibitive.

Consider that the quantity X is to be estimated from noisy observations z_k through the observation model $z_k = X + n_k$, where n_k is the observation noise. Often the noise sequence is assumed to be white (independent noise variables), stationary, zero-mean, and Gaussian. The variance of n_k is σ_n^2. The optimum maximum likelihood estimator is

$$\widehat{X} = \frac{1}{N}\sum_{i=1}^{N} z_k \qquad (1)$$

with N denoting the number of independent observations. This estimator is unbiased and has variance $\sigma_X^2 = \sigma_n^2/N^2$. Let L be the confidence interval with confidence level $1-\alpha$, that is

$$\text{Prob}\{X - L/2 \leq \widehat{X} \leq X + L/2\} = 1 - \alpha \qquad (2)$$

leading to

$$\frac{1}{\sqrt{2\pi\sigma_X^2}} \int_{-L/2}^{L/2} \exp\left(-\frac{x^2}{2\sigma_X^2}\right) dx = 1 - \alpha \qquad (3)$$

or $\alpha = 2Q(L/(2\sigma_X))$, where $Q(\cdot)$ is the complementary error function

$$Q(x) = \frac{1}{\sqrt{2\pi}} \int_x^\infty \exp(-y^2/2)\, dy \qquad (4)$$

Finally, one obtains

$$N > \frac{2\sigma_n}{L} Q^{-1}\left(\frac{\alpha}{2}\right) \qquad (5)$$

which shows that the minimum number of observations (or Monte Carlo runs) grows with the standard deviation of the observations. It increases also with the inverse of the confidence interval and the inverse of α. For instance, if $\alpha = 0.05$ (95% confidence level) the rule is $N > 3.94(\sigma_n/L)$. In practical cases the observations variance may not be known but may be estimated from the observations.

Due to the scarcity of the available simulation time I proceeded as follows. Consider that the receiver performance variable X is to be evaluated with regard to the input parameter S which takes values in the interval $[S_l, S_u]$. In each run k, a new value of S is generated using the formula

$$S_k = (1 - u_k)S_l + u_k S_u, \quad k = 1, 2, \ldots, K \qquad (6)$$

where each $u_k \in [0, 1]$ is an independent uniformly-distributed random variable. Thus, S_k is uniformly distributed in the interval $[S_l,S_u]$

The interval $[S_l, S_u]$ is then divided into a predefined number M of sub-intervals (with $M \ll K$). In each sub-interval I_m, $m = 1, \ldots, M$, the corresponding estimate $\widehat{X}(m)$ is computed by averaging the estimates $\widehat{X}_k$ that fall within I_m. The advantage of this procedure is that the simulation program can be stopped at any time (to be possibly resumed later) with the user being able to estimate the behavior of the receiver performance variable X along the whole interval $[S_l, S_u]$. Obviously, as more observations become available the accuracy of the estimates $\widehat{X}(m)$ is improved according to (5). This procedure is quite convenient for simulation parallelization where different PCs operate in parallel with the same program but using distinct noise "seeds". The merge of the partial results permits to build a plot of $X(S)$ with the desired accuracy.

3.2. Simulation Process

The simulation process is divided in this section into two important steps:

- **Parametrization and simulation**: where the parameters to be tested are defined

Variable	F=fixed, T=tested	Value	Units
$\text{Time}_{\text{simulation}}$	T	[0,+∞[	s
$\text{Frequency}_{\text{sampling}}$	F	58.5813	MHz
C/N_0	T	[20:50]	dB-Hz
$\text{Time}_{\text{integration}}$	T	[1,2]	ms
Early Late Spacing	T	[0.1,0.2]	T_C
B_{PLL}	F	20	Hz
ξ_{PLL}	F	0.707	adimensional
B_{DLL}	F	0.15	Hz
$\text{Frequency}_{\text{Doppler}}$	F	5000	Hz
$\text{Frequency}_{\text{Doppler+error}}$	F	5020	Hz
T_C	F	≈ 65.168	ns
$\text{Frequency}_{\text{carrier}}$	F	1.191795	GHz
$\text{Frequency}_{\text{subcarrier}}$	F	15.345	MHz
Chip Rate	F	10.23	MHz

Table 1: Table of used parameters

- **Image Generation**: where the results for the given parameters are obtained.

3.2.1 Parametrization

In this step a definition of the variable values to be tested in the signal processing phase is needed. These parameters are extensive and are summarized in table 1.

A brief explanation is presented regarding the importance and influence of each variable in the simulation process:

- **Time of Simulation**: Parameter that controls the processed signal length by extending the number of integrations made. Depending on the device, an average ratio of 1:400 (1 second of simulated signal = 400 seconds of processing real time) for each processing core is obtained.

- **Sampling Frequency**: This parameter influences the signal discretization process. The chosen value of 58.5813 MHz depends on various factors like minimum (Nyquist) sampling frequency and noise bandwidth. In our case, the combined frequencies of the subcarrier and the chipping rate result in an equivalent baseband bandwidth of $f_{BB} = f_{subc} + f_{chip} = 25.575$ MHz which dictates a Nyquist minimum sampling frequency of $2 \times 25.575 = 51.15$ MHz.

- **C/N_0**: The input GNSS signal is controlled by C/N_0 as it modifies the signal amplitude relatively to the noise amplitude (assumed constant in the simulation).

- **Time of Integration**: This parameter defines the time interval where the receiver accumulates data and influences the response speed of the receiver and robustness to noise (higher integration times permit a lower sensibility to noise but makes the receiver response to variations slower).

- **Early Late Spacing**: EL spacing controls the interval between the early and late replicas when correlating the local generated and received signals. A higher value of EL spacing will result in higher early late replicas power discrepancy and influence the discriminator output.

- **B_{PLL} and B_{DLL}**: These parameters define the equivalent noise bandwidth of the PLL and DLL respectively which influence the response time of each loop to code delay and frequency variations (higher bandwidths results in better response but exhibit higher sensibility to noise). The value of the DLL equivalent noise bandwidth may be low because the tracking algorithm is aided by the PLL (rate aided DLL). In fact, rate-aiding allows the noise bandwidth to be significant smaller. A smaller bandwidth is tolerable because any system dynamics is captured by the rate estimates from the PLL. Thus, the bandwidth of rate aided DLLs can be as low as 0.005 Hz [11]. Smaller bandwidths are prone to raise problems because the ionosphere eventually causes the receiver code delay to diverge from the carrier phase.
  The first-order DLL used in the simulations is characterized by the gain

$$G_{\mathrm{DLL}} = \gamma_c g_c \tag{7}$$

  where γ_c is an adimensional factor and g_c is the slope of the normalized discriminator response $D_{\mathrm{NELP}}(\epsilon)$ at $\epsilon = 0$ (NELP discriminator gain). The NELP discriminator gain g_c versus the E-L spacing is shown in fig. 2. For (non-rate aided) first-order DLL the noise equivalent bandwidth becomes [11]

$$B_{\mathrm{DLL}} = \frac{G_{\mathrm{DLL}}}{4} = \frac{\gamma_c g_c}{4} \tag{8}$$

- **Doppler Frequency**: Doppler frequency is related to the relative speed satellite-receiver as

$$f_D = -\frac{V f_c}{c} \tag{9}$$

  where V is the relative speed satellite-receiver, c is the speed of light, and f_c is the carrier frequency.
  With a Doppler frequency of 5000 Hz we are simulating a speed of $\approx$ 1250 m/s which translate into a constant phase and code delay decrease.

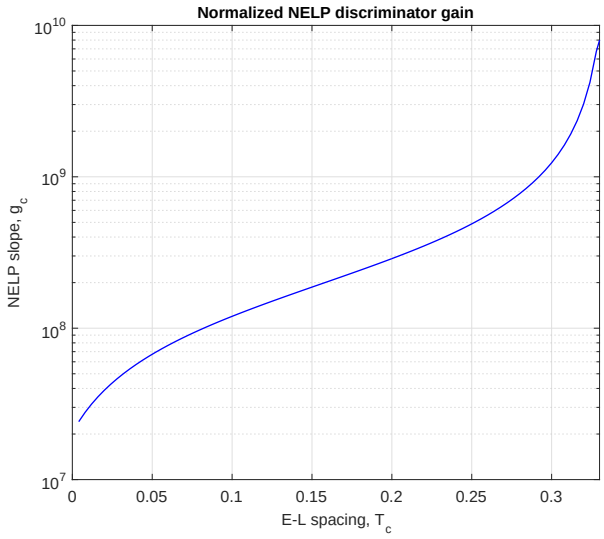

Figure 2: Normalized NELP discriminator gain versus E-L spacing

EL	0.2 T_C
CN_0	50 dB-Hz
Time of simulation	1 s
Time of Integration	2 ms

Table 2: Parameter set

- **E5 Signal constants**: The carrier and subcarrier frequency and chip rate are all characteristics of the simulated E5 AltBOC signal.

3.2.2 Plots

After the simulation process in concluded, the final step is to generate the corresponding results in the form of visual information. Specifically, the generated plots show the discriminators outputs of both the PLL and DLL and the phase and code errors along the time of simulation. The typical plots that are generated in the end are alike the ones presented in fig. 3, 4, 5 and 6 (these figures are the result of the parameter set in table 2 along with the fixed parameters displayed in table 1). These figures represent a situation where both the PLL and DLL are functioning properly with a C/N_0 of 50 dB-Hz.

Figure 3 represents the Phase discriminator output and shows the convergence of the response to 0 after a period of transition and figure 4 shows the error of the phase along the simulation around -0.625 rad or -37 degrees.

Figure 5 represents the code discriminator output and also shows the convergence of the response to 0 after a transient and figure 6 shows the error of the code along the simulation stabilizing around 0.2 m.

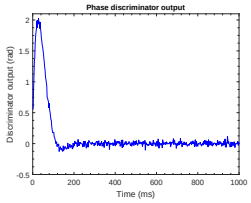

Figure 3: PLL discriminator output

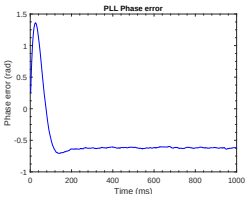

Figure 4: Phase error

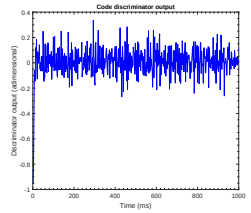

Figure 5: DLL discriminator output

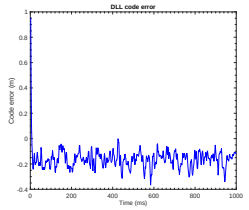

Figure 6: Code error

Figures 7, 8, 9 and 10 represent the results obtained for a C/N_0 of 50 dB-Hz where we purposely input an error to the Doppler frequency at t=600 ms and where we can observe the phase and code errors diverging. The Doppler frequency was increased by a value of 25 Hz per ms during the interval of 8 ms corresponding to a total of 200 Hz. This situation caused the PLL to lose track and induces an error to the DLL code error output. In the simulation process, the lock was considered to be lost when a phase larger than 1 rad was observed in the phase discriminator output at any time.

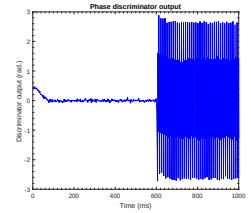

Figure 7: Phase discriminator of failed lock

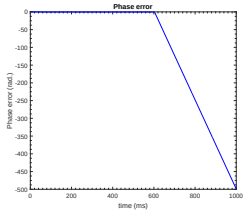

Figure 8: Phase error of failed lock

3.3. Results

The test step is composed by an iterating optimization process (where each parameter is optimized while all others are fixed) and a robustness test where the carrier-to-noise value is decreased resulting in a GNSS signal amplitude decrease. Since the receiver is simulated with random noise, the results varies in a small interval of tested parameters. To avoid this problem, in a given graph, the results are grouped by fixed length intervals and averaged

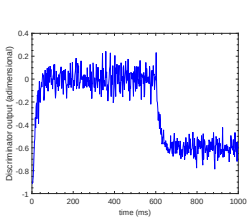

Figure 9: Code discriminator of failed lock

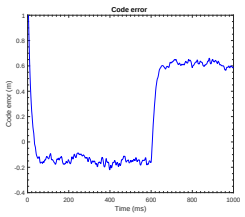

Figure 10: Code error of failed lock

in order to mitigate spiked looking graph lines. To avoid engaging in periodic phenomenon biased solutions, all parameter values are randomly chosen by a uniform distribution in a given interval, as mentioned in section 6.1.

The optimization process consists in optimizing individually each parameter. The optimized parameters are the signal sampling frequency (f_{sample}), PLL equivalent noise bandwidth (B_{PLL}) and DLL equivalent noise bandwidth (B_{DLL}). The tests were made for both the SSB and DSB to check the consistency of the chosen parameter values. The resulting optimized parameters were already shown in table 1.

The following section displays the results regarding the tests with varying C/N_0. The criterion used to detect lock failure consists in declaring loss of lock whenever the phase error exceeds 1 radian.

3.3.1 C/N_0 Variation

In this section, we present the results of testing the simulated receiver to noise for two distinct parameters: early-late spacing (EL) and integration time (T_{int}) for both SSB and DSB. Figure 11 indicates the percentage of loss of lock versus C/N_0 and fig. 12 indicates the RMS errors versus C/N_0. In both cases different values of T_{int} were considered. Keep in mind that the error values in fig. 12 correspond to the part of simulations where there was not loss of tracking.

Analyzing fig. 11 and 12, we conclude that:

- the percentage of loss of tracking is essentially independent of the bandwidth considered, SSB or DSB;
- generally, at lower C/N_0, T_{int}=2 ms presents better results for both SSB and DSB than T_{int}=1 ms with respect to loss of tracking;
- the DSB simulation presents better code error values;
- for C/N_0 <25 dB-Hz, the variance of the error is high because in this interval the tracking

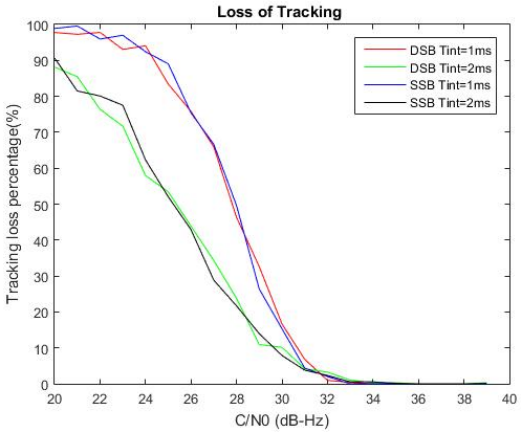

Figure 11: Loss of tracking of SSB and DSB for T_{int}=[1,2] ms

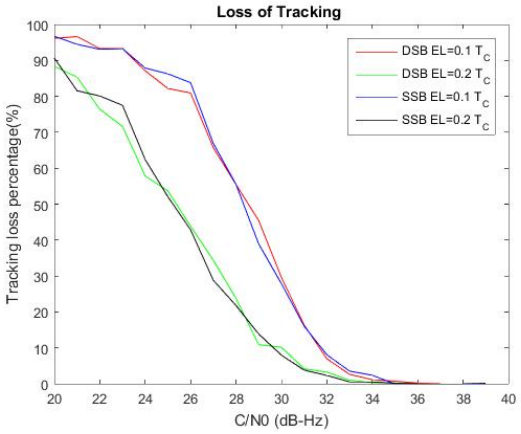

Figure 13: Loss of tracking of SSB and DSB for EL=[0.1,0.2] T_C

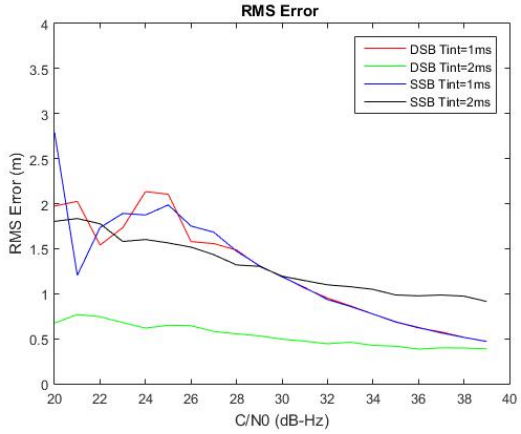

Figure 12: RMS error of successful trackings for SSB and DSB for T_{int}=[1,2] ms

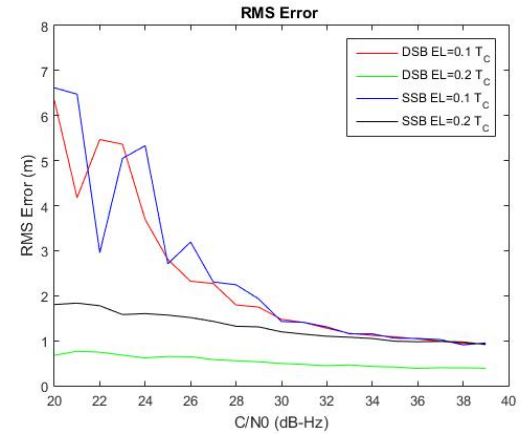

Figure 14: RMS error of successful trackings for SSB and DSB for EL=[0.1,0.2] T_C

loss is almost certain (100%) which permits to recover only a few valid error values;

- for higher values of C/N_0 a time of integration of 1 ms is better than 2 ms when comparing the average error;
- for $C/N_0 > 31$ dB-Hz approximately, the probability of track loss is $< 10\%$ for both bands and integration time tested.

Figures 13 and 14 indicate, respectively, the percentage of loss of tracking and RMS errors versus C/N_0 obtained with different values of early-late spacing. The early-late spacing parameter has influence when correlating the local signal replica and the receiver signal. By analyzing figures 13 and 14 we can conclude that:

- generally EL=0.2 T_C presents better results for both SSB and DSB than EL=0.1 T_C at all C/N_0 except for SSB at high C/N_0 which seemed independent;
- the DSB simulation presents better code error values;
- for C/N_0 <25 dB-Hz, the variance of the error is high because in this interval the tracking loss is almost certain (100%) which permits to recover only a few valid error values.

3.4. Interference Test

This section is part of the paper accepted for presentation in the ICL-GNSS2016 conference [12].

Current Global Navigation Satellite Systems use spread-spectrum modulation schemes but, due to the weak power of the received signals at the earth surface, they can be easily disturbed or even destroyed in the presence of certain types of RFI (radio frequency interference) which are intentionally provoked (jamming) or are due to the proximity of authorized radio sources, such as TV/FM, radar, navigation and mobile systems [3]. In general, non-intentional RFI is provoked by narrowband continuous or pulsed signals whereas jamming is caused by

wideband transmitters using frequency modulated chirp signals. We assume that the received signal $r(t)$ is disturbed by the additive RFI waveform

$$s(t) = A_J \cos(\varphi_J(t)) \tag{10}$$

with the interference-to-noise power being $C_I N_0 = A_J^2/(2N_0)$. Two types of continuous interferers are considered: a sinusoidal waveform of frequency $f_0 + f_J$, with f_J accounting for the jammer's frequency offset regarding the GNSS carrier frequency, and a chirp waveform, with period of repetition T_J, described by

$$\varphi_J(t) = 2\pi(f_0 - W/2)\tau(t) + \pi\gamma_J\tau^2(t) + \varphi_0. \tag{11}$$

W stands for the frequency sweep range, $\gamma_J = W/T_J$ and $\tau(t) = \mathrm{mod}(t, T_J)$ is the remaining part after division of t by T_J with $0 \le \tau(t) < T_J$. The instantaneous frequency $(2\pi)^{-1}(d\varphi_J(t)/dt)$, centered at the carrier frequency f_0, is sketched in fig. 15.

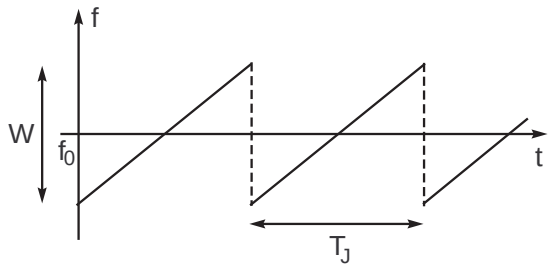

Figure 15: Frequency sweep of the chirp jamming signal.

Figures 16 and 17 illustrate the mechanism of loss of phase and code tracking due to the introduction of a sinusoidal signal of interference with frequency $f_J = 1$ MHz at time $t = 0.15$ s. The carrier-to-noise density ratio due to thermal noise is $(C/N_0) = 50$ dB-Hz and the interference-to-noise density ratio is $(C_I/N_0) = 95$ dB-Hz. The correlation interval is $T = 2$ millisecond and the adopted sampling rate is 58.52 Msamples/s which corresponds to 5.72 samples per chip. The PLL filter parameters are $a = 1348$ and $b = 52$, which corresponds to a loop bandwidth $B_n = 20$ Hz and damping factor $\xi = 0.71$. The early-late spacing of the normalized NELP discriminator is made equal to $0.2T_c$ yielding a gain $g_c = 3 \times 10^8$/s. The loop gain γ_c is 2×10^{-9} producing a DLL bandwidth of 0.15 Hz. In all the simulations we considered a Doppler frequency of 5 kHz.

The effective signal carrier-to-noise density ratio [1]

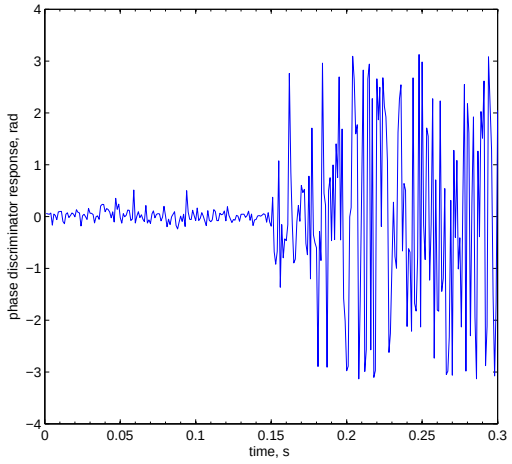

Figure 16: Example of PLL phase discriminator response in radians in the presence of sinusoidal interference

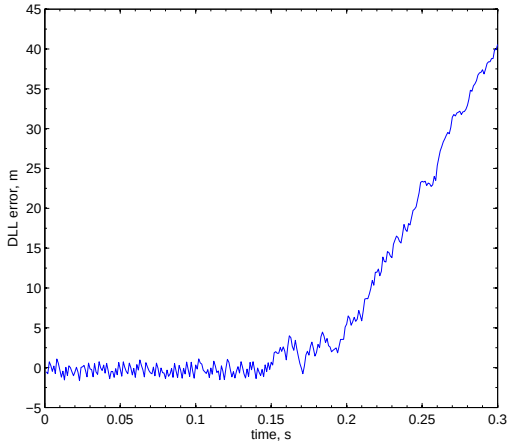

Figure 17: Example of DLL code error in meters in the presence of sinusoidal interference

$$\left(\frac{C}{N_0}\right)_{\text{eff}} = \left(\frac{C}{N_0}\right) \frac{\eta}{1 + \left(\frac{C_I}{N_0}\right)\frac{k_{\text{ssc}}}{\eta}} \tag{12}$$

is a useful way to quantify the effect of the interference on the quality of the received signal. In (12),

$$\eta = \int_{-B}^{B} G_s(f)\, df < 1 \tag{13}$$

is the fraction of signal power passed by the precorrelation bandwidth. Parameter k_{ssc} is the spectral separation coefficient (SSC) defined by

$$k_{\text{ssc}} = \int_{-B}^{B} G_I(f) G_s(f)\, df \tag{14}$$

where $2B$ is the RF bandwidth, $G_I(f)$ is the normalized interference power spectrum and $G_s(f)$ is the AltBOC signal normalized power.

Equations (12) and (14) show that the reduction of $(C/N_0)_{\text{eff}}$ for a given value of C_I/N_0) depends on the SSC. For narrowband (sinusoidal) interference with frequency f_J the interference power spectrum is $G_I(f) = (1/2)[\delta(f + f_J) + \delta(f - f_J)]$ and the SSC is given by $k_{\text{ssc}} = G_s(f_J)$. Therefore, the receiver's resistance to RFI depends on the frequency f_J with maximum robustness being expected when f_J is close to a null of $G_s(f)$ (the first positive minima of $G_s(f)$ occur at 5.115 MHz and 25.57 MHz). This behavior is corroborated by Monte Carlo simulations carried out with full band and with upper sub-band signal processing, as shown in fig. 18. The figure presents the smallest values of (C_I/N_0) (averaged over 25 independent runs) which lead to the loss of lock of the DLL/PLL. We adopted the PLL discriminator output exceeding 1 radian as the criterion for the loss of lock. Near the spectrum nulls we note an increase of the receiver robustness to interference. On the other hand, the minimum of robustness to RFI is obtained at the frequency corresponding to the maximum of the power spectrum which is approximately 15 MHz.

The upper sub-band signal processing still uses the structure of fig. 1 but now the reference signals $\widetilde{I}(t)$ and $\widetilde{Q}(t)$ are simplified to

$$\widetilde{I}(t) = -e_{E5b-Q}(t)\text{sc}_{E5-S}(t - T_s/4) \quad (15)$$

$$\widetilde{Q}(t) = e_{E5b-Q}(t)\text{sc}_{E5-S}(t) \quad (16)$$

Since the power contained in the upper sub-band is only half the full-band power, the receiver exhibits a smaller immunity against interference, as shown in the figure (dashed line). The degradation is around 6 dB.

Consider now wideband RFI. It can be shown [7] that the line power spectral density of the chirp interference is approximately rectangular with bandwidth W, provided that $WT_J \gg 1$. Taking into account the rectangular approximation to the RFI power spectrum, the SSC is well approximated by

$$k_{\text{ssc}} \approx \frac{1}{W}\int_{-W/2}^{W/2} G_s(f)\, df \quad (17)$$

with the plot being displayed in fig. 19.

The simulation results of Fig. 20 were plotted using two different chirp repetition periods: $T_J = 20\,\mu$s and $200\,\mu$s. The figure shows that the robustness to interference is maximum in the region with $W < 20$ MHz, which corresponds to the SSC minimum both for full-band and upper sub-band processing.

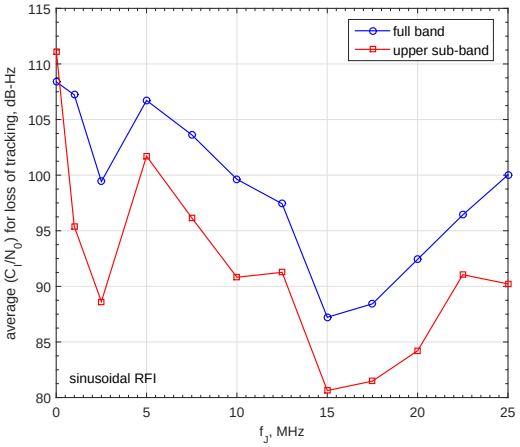

Figure 18: Average (C_I/N_0) for loss of tracking with full band and upper sub-band processing for sinusoidal interference

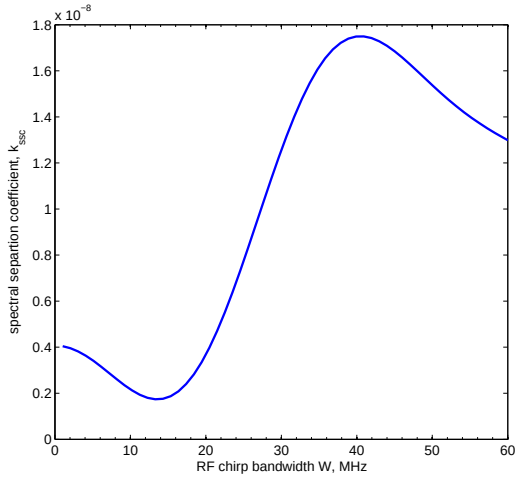

Figure 19: Spectral separation coefficient versus the RF chirp signal bandwidth

In Fig. 20 we found a loss of robustness of about 6 dB when half-band processing replaces the full-band processing because the power of the incoming signal is decreased by half. Also, there is no clear difference in the receiver's performance between the two chirp repetition periods, T_J, for $W < 25$ MHz, but above that value the receiver becomes less robust to the interference with smaller value of T_J.

In general, the pattern of robustness for the chirp RFI follows relatively well the evolution of the SSC parameter plotted in Fig. 19. In fact, the maximum of robustness is achieved at low values of W and starts to diminish for $W > 15$ MHz which corresponds to the positive slope of the SSC plot. The minimum of robustness is achieved at $W \approx 35$ MHz which corresponds approximately to the maximum of the SSC curve.

Simulations have shown that the performance degradation due to radio frequency interference is well predicted by SSC both for the narrowband and the wideband interference signals under test. In the case of the chirp interference, the SSC value depends both on the power spectral density of the modulated signal and the frequency range of the interfering signal. However, the dependency on the rate of frequency variation is not clearly identified in the SSC parameter. Simulations have shown that, for large chirp bandwidths, the rate of frequency variation is also important with the receiver being more robust to large repetition periods of the chirp interference.

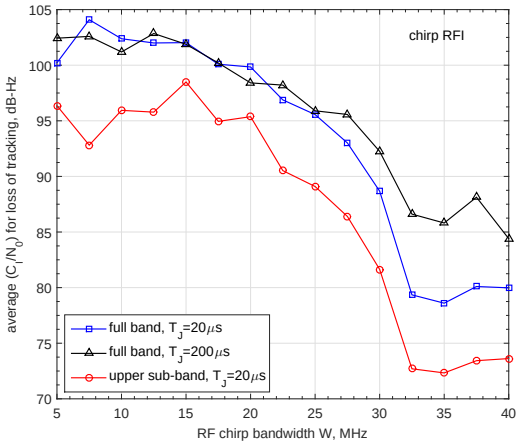

Figure 20: Average (C_I/N_0) for the loss of tracking with full band and upper sub-band processing for chirp interference

4. Conclusions

4.1. Conclusions

AltBOC is the most sophisticated of all the signals broadcast by the current GNSSs. It conveys four components and can be treated as a wideband single signal or as two independent narrowband signals. Therefore multiple solutions for the receiver architecture are possible, and the receiver implementation is still today a challenging task.

The implementation of this thesis corresponded to a period of intense learning of the technical aspects by the candidate, concerning the AltBOC modulation. With this thesis the candidate had several objectives in mind: (i) gain insight into the nature of the AltBOC modulation, (ii) analyze the different aspects in the implementation of AltBOC receivers, (iii) implement and test distinct receiver architectures, namely Single Sideband and Double Sideband processing, and compare their results. From the resulting work, the final remarks are summarized:

- Given the differences of the AltBOC modulation relative to other less sophisticated modulations, like BPSK, an extensive theoretical study regarding the DSB and SSB E5 AltBOC signal receiver architectures was presented;
- A functional receiver was implemented for both SSB and DSB processing;
- The DSB processing presents better results in terms of average positioning error for all C/N_0;
- Several receiver parameters were discussed and optimized. Namely the Early-Late spacing and time of integration were tested and results were shown.
- It was concluded that higher values of time of integration result in better results of robustness to noise for lower C/N_0;
- For the E-L spacing the value of 0.2 T_C presents better results both for the average error and robustness than 0.1 T_C. Higher values of E-L spacing are not advised since the linear region of the NELP discriminator response is reduced which could increase the probability of false-lock synchronization;
- Interference tests were proposed and simulation results were presented in chapter 6. A conference paper was produced and accepted for presentation with the results obtained in this topic [12];
- A simulation paralelization procedure was developed where the tested variable was chosen randomly in an uniformly distributed interval. The results were grouped in a pre-defined number of sub-intervals and averaged. This procedure permitted to accelerate the simulation process by resorting to multiple computers.

4.2. Future work

Although falling outside the scope of the present work, the following points are interesting topics to reveal the potentialities of the AltBOC receiver architectures:

- Test the algorithms with real satellite data;
- Compare the Dual Sideband and Single Sideband results with the BPSK-R(10) approach;
- Test the AltBOC receiver architectures in multipath scenarios;
- Analyze the effects and test the implemented receivers using a finite number of quantization levels;
- Implement the acquisition algorithm which due to its complexity, was not addressed in this work.

References

[1] J. W. Betz and K. R. Kolodziejski. Generalized theory of code tracking with an early-late discriminator, part ii: Noncoherent processing and numerical results. *IEEE Transactions on Aerospace and Electronic Systems*, 45(4):1551–1564, October 2009.

[2] I. Colomina et al. The accuracy potential of Galileo E5/E1 pseudoranges for surveying and mapping. In *Proceedings of ION GNSS 2011*, pages 2332–2340, September 2011.

[3] F. Dovis, editor. *GNSS Interference Threats and Countermeasures*. Artech House, 2015.

[4] G. X. Gao et al. Ionosphere effects for wideband GNSS signals. In *Proceedings of ION Annual Meeting 2007*, pages 147–155, April 2007.

[5] N. Gerein. Hardware architecture for processing Galileo alternate binary offset carrier (AltBOC) signals. patent US2005/0012664 A1, January 2005.

[6] M. C. Jeruchim, P. Balaban, and K. S. Shanmugan, editors. *Simulation of Communication Systems. Modeling, Methodology and Techniques*. Kluwer, 2000.

[7] J. Klauder, A. Price, S. Darlington, and W. Albersheim. The theory and design of chirp radars. *The Bell System Technical Journal*, 34(4):745–808, July 1960.

[8] L. Lestarquit, G. Artaud, and J.-L. Issler. AltBOC for dummies or everything you always wanted to know about AltBOC. In *Proceedings of ION 2008 GNSS*, pages 961–970, September 2008.

[9] D. Margaria. *Galileo AltBOC Receivers*. PhD thesis, Politecnico di Torino, Italy, July 2007.

[10] D. Margaria et al. An innovative data demodulation technique for Galileo AltBOC receivers. *Journal of Global Positioning Systems*, 6(1):89–96, 2007.

[11] P. Misra and P. Enge. *Global Positioning System: Signals, Measurements and Performance*. Ganga-Jamuna Press, 2006.

[12] F. D. Nunes, R. F. D. Nunes, and F. M. G. Sousa. Performance evaluation in AltBOC receivers affected by interference. In *Proceedings of ICL-GNSS2016*, pages 1–6, June 2016.

[13] N. C. Shivaramaiah. *Enhanced Receiver Techniques for Galileo E5 AltBOC Signal Processing*. PhD thesis, University of South Wales, Sydney, Australia, June 2011.

[14] J.-M. Sleewaegen, W. D. Wilde, and M. Hollreiser. Galileo AltBOC receiver. In *Proceedings of European Navigation Conference 2004*, pages 1–9, May 2004.

[15] M. Soellner. Comparison of awgn code tracking accuracy for alternative-BOC, complex-LOC and complex-BOC modulation options in Galileo E5-band. In *Proceedings of the European Navigation Conference ENC-GNSS 2003*, April 2003.

[16] H. Tokura et al. The possibility of precise automobile navigation using GPS/QZSS L5 and Galileo E5 pseudoranges. In *Proceedings of ION ITM 2013*, pages 194–202, January 2013.

[17] J. vila Rodrguez. *On Generalized Signal Waveforms for Satellite Navigation*. PhD thesis, Universitat der Bundeswehr, Munich, June 2008.

[18] W. D. Wilde, J.-M. Sleewaegen, and G. Seco-Granados. A method and device for demodulating Galileo alternate binary offset carrier (AltBOC) signals. patent 2006027004 A1, March 2006.